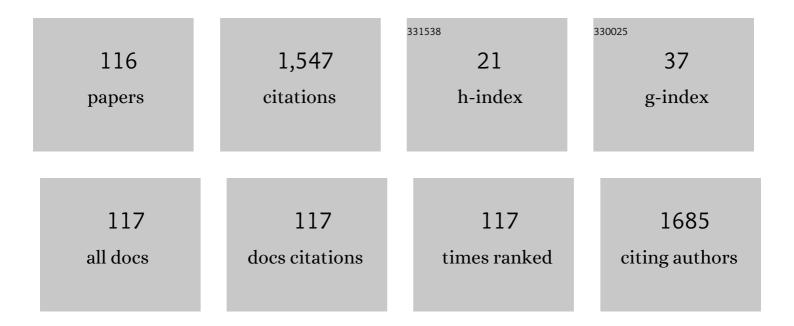
Masashi Arita

List of Publications by Year in descending order

Source: https://exaly.com/author-pdf/6513317/publications.pdf Version: 2024-02-01



#	Article	IF	CITATIONS
1	Giant tunneling magnetoresistance in epitaxial Co2MnSi/MgO/Co2MnSi magnetic tunnel junctions by half-metallicity of Co2MnSi and coherent tunneling. Applied Physics Letters, 2012, 101, .	1.5	219
2	Spin-dependent tunneling characteristics of fully epitaxial magnetic tunneling junctions with a full-Heusler alloy Co2MnSi thin film and a MgO tunnel barrier. Applied Physics Letters, 2006, 89, 192505.	1.5	182
3	Fabrication of fully epitaxial magnetic tunnel junctions using cobalt-based full-Heusler alloy thin film and their tunnel magnetoresistance characteristics. Journal Physics D: Applied Physics, 2006, 39, 824-833.	1.3	93
4	<i>In situ</i> transmission electron microscopy analysis of conductive filament during solid electrolyte resistance switching. Applied Physics Letters, 2011, 98, .	1.5	76
5	Switching operation and degradation of resistive random access memory composed of tungsten oxide and copper investigated using in-situ TEM. Scientific Reports, 2015, 5, 17103.	1.6	60
6	Resistance switching properties of molybdenum oxide films. Thin Solid Films, 2012, 520, 4762-4767.	0.8	45
7	Tungsten Films with the A15 Structure. Japanese Journal of Applied Physics, 1993, 32, 1759-1764.	0.8	42
8	Effect of nonstoichiometry on the half-metallic character of Co2MnSi investigated through saturation magnetization and tunneling magnetoresistance ratio. Physical Review B, 2014, 89, .	1.1	42
9	Fabrication of Fe-doped WO3 films for NO2 sensing at lower operating temperature. Sensors and Actuators B: Chemical, 2015, 221, 393-400.	4.0	42
10	Thin film deposition and characterization of pure and iron-doped electron-beam evaporated tungsten oxide for gas sensors. Thin Solid Films, 2010, 518, 4791-4797.	0.8	41
11	Filament formation and erasure in molybdenum oxide during resistive switching cycles. Applied Physics Letters, 2014, 105, .	1.5	41
12	Structural and magnetic properties of epitaxially grown full-Heusler alloy Co2MnGe thin films deposited using magnetron sputtering. Journal of Applied Physics, 2006, 99, 08J110.	1.1	31
13	Improved tunnel magnetoresistance characteristics of magnetic tunnel junctions with a Heusler alloy thin film of Co2MnGe and a MgO tunnel barrier. Journal of Applied Physics, 2007, 101, 09J513.	1.1	29
14	The effect of pressure and W-doping on the properties of ZnO thin films for NO2 gas sensing. Applied Surface Science, 2015, 357, 728-734.	3.1	28
15	Probing electrochemistry at the nanoscale: in situ TEM and STM characterizations of conducting filaments in memristive devices. Journal of Electroceramics, 2017, 39, 73-93.	0.8	28
16	I-V measurement of NiO nanoregion during observation by transmission electron microscopy. Journal of Applied Physics, 2011, 109, 053702.	1.1	25
17	Determination of Long-Range-Order Parameter of Fe ₃ Si Alloy by means of ⁵⁷ Fe Mössbauer Effect. Transactions of the Japan Institute of Metals, 1985, 26, 710-720.	0.5	24
18	Transmission electron microscopy of La0.7Ca0.3MnO3 thin films. Journal of Magnetism and Magnetic Materials, 2000, 211, 84-90.	1.0	22

Masashi Arita

#	Article	IF	CITATIONS
19	In-situ transmission electron microscopy of conductive filaments in NiO resistance random access memory and its analysis. Journal of Applied Physics, 2013, 113, 083701.	1.1	22
20	Development of TEM Holder Generating In-Plane Magnetic Field Used for <i>In-Situ</i> TEM Observation. Materials Transactions, 2014, 55, 403-409.	0.4	22
21	Smooth Interfacial Scavenging for Resistive Switching Oxide via the Formation of Highly Uniform Layers of Amorphous TaO _{<i>x</i>} . ACS Applied Materials & Interfaces, 2018, 10, 5609-5617.	4.0	22
22	Preparation of resistance random access memory samples for in situ transmission electron microscopy experiments. Thin Solid Films, 2013, 533, 48-53.	0.8	20
23	Analysis of resistance switching and conductive filaments inside Cu-Ge-S using in situ transmission electron microscopy. Journal of Materials Research, 2012, 27, 886-896.	1.2	19
24	Switching of Cu/MoO <i>_x</i> /TiN CBRAM at MoO <i>_x</i> /TiN interface. Physica Status Solidi (A) Applications and Materials Science, 2016, 213, 306-310.	0.8	17
25	Microstructural transitions in resistive random access memory composed of molybdenum oxide with copper during switching cycles. Nanoscale, 2016, 8, 14754-14766.	2.8	17
26	Multifunctional Device Using Nanodot Array. Japanese Journal of Applied Physics, 2006, 45, 5317-5321.	0.8	16
27	Epitaxial growth of Heusler alloy Co2MnSi/MgO heterostructures on Ge(001) substrates. Applied Physics Letters, 2011, 98, 262505.	1.5	16
28	The Observation of "Conduction Spot―on NiO Resistance Random Access Memory. Japanese Journal of Applied Physics, 2011, 50, 081101.	0.8	15
29	Single-Electron Device With Si Nanodot Array and Multiple Input Gates. IEEE Nanotechnology Magazine, 2009, 8, 535-541.	1.1	13
30	Highly Spin-Polarized Tunneling in Epitaxial Magnetic Tunnel Junctions with a Co ₂ MnSi Electrode and a MgO Barrier with Improved Interfacial Structural Properties. Japanese Journal of Applied Physics, 2012, 51, 093004.	0.8	13
31	Green Synthesis of Size-Tunable Iron Oxides and Iron Nanoparticles in a Salt Matrix. ACS Sustainable Chemistry and Engineering, 2019, 7, 17697-17705.	3.2	12
32	Tip production technique to form ferromagnetic nanodots. Materials Science and Engineering C, 2003, 23, 927-930.	3.8	11
33	In situConductance Measurement of a Limited Number of Nanoparticles during Transmission Electron Microscopy Observation. Japanese Journal of Applied Physics, 2005, 44, L790-L792.	0.8	11
34	(Invited) Visualization of Conductive Filament of ReRAM during Resistive Switching by in-situ TEM. ECS Transactions, 2015, 69, 299-309.	0.3	11
35	Microstructure and electric property of MgO/Fe/MgO tri-layer films forming a nano-granular system. Microelectronic Engineering, 2008, 85, 2445-2450.	1.1	10
36	The Observation of "Conduction Spot―on NiO Resistance Random Access Memory. Japanese Journal of Applied Physics, 2011, 50, 081101.	0.8	10

#	Article	IF	CITATIONS
37	Crystal structures and light absorption spectra of 1,4â€dithioketoâ€3,6â€diphenylâ€pyrroloâ€{3,4â€e]â€pyrrole. Journal of Applied Physics, 1991, 70, 4065-4072.	1.1	9
38	The electron-density distribution and chemical bonding of A15-type Cr obtained by the maximum-entropy method. Journal of Physics Condensed Matter, 1994, 6, 8681-8690.	0.7	9
39	Structural and electromagnetic characterizations of Fe–SrF2granular films. Journal Physics D: Applied Physics, 2006, 39, 5103-5108.	1.3	9
40	In Situ TEM Observation of Cu/MoOx ReRAM Switching. ECS Transactions, 2013, 58, 19-25.	0.3	8
41	A new crystal structure of 3,6-diphenylpyrrolo[3,4-c]pyrrole-1,4-dithione. Acta Crystallographica Section C: Crystal Structure Communications, 1991, 47, 1952-1956.	0.4	7
42	Tunnel current measurement of MgO and MgO/Fe/MgO nanoregions during TEM observation. Superlattices and Microstructures, 2008, 44, 633-640.	1.4	7
43	Fabrication of double-dot single-electron transistor in silicon nanowire. Thin Solid Films, 2010, 518, S186-S189.	0.8	7
44	Periodic Coulomb blockade oscillations observed in single-layered Fe nanodot array. Thin Solid Films, 2020, 704, 138012.	0.8	7
45	Stable and Tunable Current-Induced Phase Transition in Epitaxial Thin Films of Ca2RuO4. ACS Applied Materials & Interfaces, 2020, 12, 28368-28374.	4.0	7
46	Crystal structure of the ordered Nb10Ge7 phase. Journal of Solid State Chemistry, 1990, 84, 386-400.	1.4	6
47	Single-electron transistor properties of Fe–SrF2 granular films. Materials Science and Engineering B: Solid-State Materials for Advanced Technology, 2008, 147, 100-104.	1.7	6
48	Fabrication and single-electron-transfer operation of a triple-dot single-electron transistor. Journal of Applied Physics, 2015, 118, .	1.1	6
49	Fabrication and evaluation of series-triple quantum dots by thermal oxidation of silicon nanowire. AIP Advances, 2015, 5, .	0.6	6
50	Coupling capacitance between double quantum dots tunable by the number of electrons in Si quantum dots. Journal of Applied Physics, 2015, 117, .	1.1	6
51	Visualization of Conductive Filament during Write and Erase Cycles on Nanometer-Scale ReRAM Achieved by In-Situ TEM. , 2015, , .		6
52	Observation of Conductive Filament in CBRAM at Switching Moment. ECS Transactions, 2017, 80, 895-902.	0.3	6
53	Morphological study of Cr smoke particles with A15 structure. Philosophical Magazine A: Physics of Condensed Matter, Structure, Defects and Mechanical Properties, 2001, 81, 1597-1612.	0.7	5
54	Silicon nanodot-array device with multiple gates. Materials Science in Semiconductor Processing, 2008, 11, 175-178.	1.9	5

Masashi Arita

#	Article	IF	CITATIONS
55	Smoke particles of ytterbium and its oxides. Journal of Crystal Growth, 1993, 132, 71-81.	0.7	4
56	Transmission electron microscopy of La0.7Ca0.3 MnO3 CMR films. Journal of Electron Microscopy, 1999, 48, 381-385.	0.9	4
57	Conductance measurements of nanoscale regions with in situ transmission electron microscopy. Materials Science and Engineering C, 2006, 26, 776-781.	3.8	4
58	Surface magnetic structure of epitaxial magnetite thin films grown on MgO(001). Journal of Applied Physics, 2009, 105, 07D545.	1.1	4
59	(Invited) High-Speed Operation of Si Single-Electron Transistor. ECS Transactions, 2013, 58, 73-80.	0.3	4
60	Initial states and analog switching behaviors of two major tantalum oxide resistive memories. Japanese Journal of Applied Physics, 2020, 59, 044004.	0.8	4
61	Charge-offset stability of single-electron devices based on single-layered Fe nanodot array. AIP Advances, 2021, 11, .	0.6	4
62	Electron microscopy of phase boundaries between the A15 and D8 _m , structures of Nb-ge. Philosophical Magazine Letters, 1989, 60, 161-169.	0.5	3
63	DEFECTS OF A15 SMALL PARTICLES IN TUNGSTEN THIN FILMS. Surface Review and Letters, 1996, 03, 1191-1194.	0.5	3
64	Magnetic microstructure of NiFe/Cu/NiFe films observed by Lorentz microscopy. Journal of Electron Microscopy, 1999, 48, 595-600.	0.9	3
65	Single-electron device using Si nanodot array and multi-input gates. , 2006, , .		3
66	Filamentary switching of ReRAM investigated by in-situ TEM. Japanese Journal of Applied Physics, 2020, 59, SG0803.	0.8	3
67	Molecular Orientations of 1,4-dithioketo-3,6-diphenyl-pyrrolo-[3,4-c]-pyrrole on Crystalline Substrates. Japanese Journal of Applied Physics, 1993, 32, 2842-2853.	0.8	2
68	Effect of Arrangement of Input Gates on Logic Switching Characteristics of Nanodot Array Device. IEICE Transactions on Electronics, 2012, E95.C, 865-870.	0.3	2
69	In Situ Transmission Electron Microscopy for Electronics. , 0, , .		2
70	Capacitance evaluation of compact silicon triple quantum dots by simultaneous gate voltage sweeping. Journal of Applied Physics, 2016, 120, 234502.	1.1	2
71	Analog memory characteristics of 1T1R MoOx resistive random access memory. , 2016, , .		2
72	In-situElectron Microscopy of Cu Movement in MoOx/Al2O3Bilayer CBRAM during Cyclic Switching. ECS Transactions, 2017, 80, 903-910.	0.3	2

#	Article	IF	CITATIONS
73	Oxygen Distribution around Filament in Ta-O Resistive RAM Fabricated Using 40 nm CMOS Technology. , 2018, , .		2
74	Tunnel magnetocapacitance in Fe/MgF2 single nanogranular layered films. Applied Physics Letters, 2020, 116, .	1.5	2
75	Full Adder Operation Based on Si Nanodot Array Device with Multiple Inputs and Outputs. International Journal of Nanotechnology and Molecular Computation, 2009, 1, 58-69.	0.3	2
76	Scanning Tunneling Microscopy in Liquid on Geometrical Study of Cu(001) Surface. Japanese Journal of Applied Physics, 1995, 34, 6210-6213.	0.8	1
77	Electron microscopy of grain boundaries of Nb3Ge with the A15 structure. Physica Status Solidi A, 1996, 157, 379-392.	1.7	1
78	Microstructure of Fe/Cu (Au) artificial superlattice. Thin Solid Films, 1998, 318, 180-185.	0.8	1
79	Epitaxial growth of Fe nanodots on SrF2/Si (111). Materials Science and Engineering C, 2006, 26, 1146-1150.	3.8	1
80	Tunnel Conductance through One or a Few Fe Particles Embedded in an MgO Matrix. Japanese Journal of Applied Physics, 2006, 45, 1946-1949.	0.8	1
81	Magnetoresistance of Fe–SrF2 single-electron devices with a current-in-plane geometry. Superlattices and Microstructures, 2008, 44, 449-456.	1.4	1
82	High-frequency properties of Si single-electron transistor. , 2012, , .		1
83	Real-time resistive switching of Cu/MoOx ReRAM observed in transmission electron microscope. , 2014, , .		1
84	EELS Analysis of Oxygen Scavenging Effect in a Resistive Switching Structure of Pt/Ta/SrTiO3/Pt. MRS Advances, 2018, 3, 1925-1930.	0.5	1
85	Nanoscale filaments in Ta-O resistive RAM bit array: microscopy analysis and switching property. , 2019, , .		1
86	Controlled Current Transport in Pt/Nb:SrTiO ₃ Junctions via Insertion of Uniform Thin Layers of TaO _x . Physica Status Solidi - Rapid Research Letters, 2019, 13, 1900136.	1.2	1
87	Initial electrical properties of tantalum oxide resistive memories influenced by oxygen defect concentrations. Japanese Journal of Applied Physics, 2021, 60, SCCE03.	0.8	1
88	In-situ TEM of Nanoscale ReRAM Devices. Vacuum and Surface Science, 2018, 61, 766-771.	0.0	1
89	Electron Microscopy of the "Disordered Phase" in Nb-Ge Thin Films. Journal of Solid State Chemistry, 1993, 106, 427-442.	1.4	0
90	Electron Microscopy of Planar Defects in A15 Nb3Ge. Journal of Solid State Chemistry, 1993, 107, 76-92.	1.4	0

#	Article	IF	CITATIONS
91	Phase boundaries between A15 and D88 structures of the Nb-Ge compound system. Philosophical Magazine A: Physics of Condensed Matter, Structure, Defects and Mechanical Properties, 1993, 67, 1129-1141.	0.7	0
92	Electron Microscopy of La0.7Ca0.3MnO3. Japanese Journal of Applied Physics, 2005, 44, 304-308.	0.8	0
93	Full adder operation based on Si nanodot array device. , 2008, , .		0
94	(Invited) In Situ Transmission Electron Microscopy Analysis of Conductive Filament in Resistance Random Access Memories. ECS Transactions, 2011, 41, 81-92.	0.3	0
95	Si Nanodot Device Fabricated by Thermal Oxidation and their Applications. Key Engineering Materials, 2011, 470, 175-183.	0.4	0
96	In-Situ Transmission Electron Microscopy Observation of Electromigration in Au Thin Wires. Journal of Nanoscience and Nanotechnology, 2012, 12, 8741-8745.	0.9	0
97	Multifunctional Logic Gate by Means of Nanodot Array with Different Arrangements. Journal of Nanomaterials, 2013, 2013, 1-7.	1.5	0
98	Highly functional three-terminal nanodot array device with almost independent input gates. , 2014, , .		0
99	Tunable coupling capacitance of double-quantum-dot single-electron transistor with multiple gates. , 2014, , .		0
100	In-situ TEM observation of ReRAM switching. , 2014, , .		0
101	Study on lateral ReRAM by the use of in-situ TEM. , 2016, , .		0
102	Evaluation of the origin of excited states appeared in small Si single-electron transistors. , 2016, , .		0
103	Evaluation of serially coupled triple quantum dots with a compact device structure by a simultaneous voltage-sweeping method. , 2016, , .		0
104	(Invited) Evaluation of Coupled Triple Quantum Dots with Compact Device Structure. ECS Transactions, 2017, 80, 173-180.	0.3	0
105	Evaluation of multilevel memory capability of ReRAM using Ta <inf>2</inf> O <inf>5</inf> insulator and different electrode materials. , 2017, , .		0
106	Associative search using pseudo-analog memristors. , 2017, , .		0
107	EELS Analysis of Oxygen Scavenging Effect in a Resistive Switching Structure of Pt/Ta/SrTiO3/Pt – CORRIGENDUM. MRS Advances, 2018, 3, 2075-2075.	0.5	0
108	Nanoscale Switching and Degradation of Resistive Random Access Memory Studied by In Situ Electron Microscopy. , 0, , .		0

#	Article	IF	CITATIONS
109	Switching Current of Ta ₂ O ₅ -Based Resistive Analog Memories. , 2019, , .		0
110	Double-gate single-electron devices formed by single-layered Fe nanodot array. , 2020, , .		0
111	Initialization process of Cu-based WO _{<i>x</i>} conductive bridge RAM investigated via in situ transmission electron microscopy. Japanese Journal of Applied Physics, 2020, 59, SIIE01.	0.8	0
112	Probing Electrochemistry at the Nanoscale: In Situ TEM and STM Characterizations of Conducting Filaments in Memristive Devices. Kluwer International Series in Electronic Materials: Science and Technology, 2022, , 87-120.	0.3	0
113	<i>In situ</i> Transmission Electron Microscopy on the Conductance Quantization of a Fe Nano-particle System. Materia Japan, 2005, 44, 990-990.	0.1	0
114	Tungsten and Chromium Having the A15-Structure. Springer Series in Cluster Physics, 1999, , 285-294.	0.3	0
115	Investigation on Switching Operation in Resistive RAM Using In-Situ TEM. Springer Proceedings in Physics, 2017, , 205-214.	0.1	0
116	Full Adder Operation Based on Si Nanodot Array Device with Multiple Inputs and Outputs. , 0, , 131-139.		0

Full Adder Operation Based on Si Nanodot Array Device with Multiple Inputs and Outputs. , 0, , 131-139. 116